# Scattering Characteristic Extraction Method for Manmade Target Based on Target Null Theory

*Dongwei LU, Jiazhi MA, Bo PANG, Yifu GUAN, Dejun FENG*

[1]State Key Laboratory of Complex Electromagnetic Environment Effects on Electronics and Information System, National University of Defense Technology, 410073 Changsha, China

bookwormldw@foxmail, jzmanudt@163.com

Submitted June 2, 2022 / Accepted November 9, 2022 / Online first February 22, 2023

**Abstract.** *Scattering characteristic extraction is an essential part of manmade target recognition. However, if two scattering points are in adjacent pixels, scattering characteristic extraction may fail to acquire accurate polarimetric scattering matrices (PSMs) of the weak scattering points due to the contamination caused by the strong scattering points. Target null theory provides a way to solve this problem. By selecting the transmitting and receiving polarization states of radar antennas simultaneously, the echo power of a strong scattering point becomes zero and the contamination effect is avoided. In this paper, a method based on target null theory for scattering characteristic extraction is proposed. First, we optimize the transmitting and receiving polarization states of the radar antenna to suppress the intensities of the strong scattering points to highlight the positions of the weak scattering points in certain polarimetric channels. Second, to suppress the contamination effects of strong scattering points in other polarimetric channels, we establish perturbation correction equations to erase the error generated by the point spread function (PSF) among adjacent scattering points in the radar image. Finally, the solved polarimetric scattering matrices of corresponding positions are implemented for target retrieval. The electromagnetic simulation results demonstrate the effectiveness of the proposed method.*

## Keywords

Polarimetric radar, manmade target, target null theory, polarimetric scattering matrix, adjacent scattering points, point spread function

## 1. Introduction

Polarization is one of the essential properties of electromagnetic waves. A polarimetric radar system usually transmits and receives horizontal (H) and vertical (V) polarized waves to obtain the polarimetric scattering matrices (PSMs) of a radar target containing information about its geometric structure. Therefore, polarimetric radar has become a powerful approach for observing manmade targets such as aircraft, vehicles, ships and even satellites in the field of surveillance [1–5]. However, the point spread function (PSF) of strong scattering points might contaminate their surrounding pixels in radar images. The weak scattering centers adjacent to the strong scattering points cannot appear clearly in the radar image, resulting in a location estimation error, this phenomenon indicates that the extracted PSM does not belong to the corresponding scattering point. Therefore, location error threatens the accuracy of target recognition.

To achieve accurate geometric structure retrieval, the intensities of strong scattering points can be suppressed in one polarimetric channel depending on the scattering characteristics of the radar target. In [6], early studies on the relationships between the target characteristics and the polarization states of radar antennas were reviewed. It is found that the scattering characteristics of a radar target determine the elements of the PSM. The polarization states of transmitting and receiving antennas can be adjusted to acquire the maximum or minimum echo power levels of radar targets according to the numerical properties of their PSMs. When the echo power of a radar target in a certain polarimetric channel becomes zero, the polarization states of the radar antennas in the polarimetric domain or on the Poincaré sphere are points called target nulls. Target null theory can be applied to reduce the power levels of ground or sea clutter during target detection. In [7] and [8], group theory was introduced to radar polarimetry to determine the algebraic characteristics of target null theory among different polarimetric scattering matrices. Additionally, the geometric characteristics of target nulls were discussed in [9]. In practical applications, a synthetic aperture frequency-modulated continuous-wave (FM-CW) radar was used to detect targets buried in snowpack. The target nulls of snowpack were selected to suppress the background clutter in [10] and [11].

To reduce the effects of strong scattering points, a novel scattering characteristic (SaC) extraction method

DOI: 10.13164/re.2023.0091

based on target null theory is proposed in this paper, the polarization states of the transmitting and receiving antennas are selected simultaneously to suppress the strong scattering points with certain scattering characteristics. First, the transmitting and receiving polarization states of the radar are optimized to suppress the intensity levels of the strong scattering points and to highlight the weak points around the strong scattering points in one polarimetric channel. Second, to avoid the contamination effect of strong scattering points in other polarimetric channels, perturbation correction equations of the PSFs of multiple adjacent scattering centers are established and solved. Finally, the results of electromagnetic simulation are shown to prove that the proposed method is effective.

## 2. Theoretical Model

### 2.1 Strong Scattering Point Suppression

Because the proposed method in this paper is based on target null theory, it is necessary to explain its meaning. The PSM of a radar target with the H and V polarimetric basis is written as:

$$\mathbf{S}=\begin{bmatrix} s_{\mathrm{HH}} & s_{\mathrm{VH}} \\ s_{\mathrm{VH}} & s_{\mathrm{VV}} \end{bmatrix}. \tag{1}$$

For a manmade target, its PSM is symmetric, which means that $s_{\mathrm{VH}} = s_{\mathrm{HV}}$. If the polarization state of the transmitting antenna is the same as that of the receiving antenna, the echo power is defined as the receiving power in the co-polarization (CO-pol) channel. If the polarization state of the transmitting antenna is orthogonal to that of the receiving antenna, the echo power is detected from the cross-polarization (X-pol) channel. The echo power of the radar target is zero when the polarization states of transmitting/receiving antennas are selected. For the CO-pol channel, the echo power is as follows:

$$P_{\mathrm{CO}} = \left\| \mathbf{h}^{\mathrm{T}}\mathbf{S}\mathbf{h} \right\|_2^2 = 0\,. \tag{2}$$

In the X-pol channel, the echo power is :

$$P_{\text{X-pol}} = \left\| \mathbf{h}_{\perp}^{\mathrm{T}}\mathbf{S}\mathbf{h} \right\|_2^2 = 0 \tag{3}$$

where $\mathbf{h}$ and $\mathbf{h}_{\perp}$ are the Jones vectors of the transmitting and receiving antennas respectively, $\perp$ denotes orthogonality. $(\cdot)^{\mathrm{T}}$ denotes transposition and $\|\cdot\|_2$ is the 2-norm. The polarization state of the antenna is written as $\mathbf{h} = [\cos\gamma \quad \sin\gamma\, \mathrm{e}^{\mathrm{j}\delta}]^{\mathrm{T}}$. $(\gamma, \delta) \in [0,\pi/2] \times [0, 2\pi]$ are the parameters of the Jones vector. The orthogonal vector of the polarization state is $\mathbf{h}_{\perp} = [-\sin\gamma \quad \cos\gamma\, \mathrm{e}^{\mathrm{j}\delta}]^{\mathrm{T}}$. Based on (2) and (3), the target nulls in the CO-pol and X-pol channels are defined.

For example, the target null of the CO-pol channel of a trihedral reflector is acquired by solving (2):

$$\left\| \begin{bmatrix} \cos\gamma & \sin\gamma \mathrm{e}^{\mathrm{j}\delta} \end{bmatrix} \mathbf{S}_{\mathrm{Tri}} \begin{bmatrix} \cos\gamma \\ \sin\gamma \mathrm{e}^{\mathrm{j}\delta} \end{bmatrix} \right\|_2^2 = 0 \tag{4}$$

where $\mathbf{S}_{\mathrm{Tri}} = \begin{bmatrix} 1 & 0 \\ 0 & 1 \end{bmatrix}$, which represents the PSM of the trihedral reflector. From there, we acquire:

$$\cos^2\gamma + \sin^2\gamma \cdot \mathrm{e}^{2\mathrm{j}\delta} = 0 \tag{5}$$

From (5), it can be determined that $\delta = \pi/2$, $3\pi/2$ and $\gamma = \pi/4$. The target null of the CO-pol channel for the trihedral reflector is $\frac{1}{\sqrt{2}}[1 \quad \pm\mathrm{j}]^{\mathrm{T}}$. For the target null of the X-pol channel, according to (3), we acquire:

$$\left\| \begin{bmatrix} -\sin\gamma & \cos\gamma \mathrm{e}^{\mathrm{j}\delta} \end{bmatrix} \mathbf{S}_{\mathrm{Tri}} \begin{bmatrix} \cos\gamma \\ \sin\gamma \mathrm{e}^{\mathrm{j}\delta} \end{bmatrix} \right\|_2^2 = 0\,. \tag{6}$$

This equation can be written as follows:

$$-\sin\gamma\cos\gamma + \sin\gamma\cos\gamma \cdot \mathrm{e}^{2\mathrm{j}\delta} = 0\,. \tag{7}$$

Equation (7) is always valid when $\delta = 0$, which means that an arbitrary linear polarization can be the target null of the X-pol channel for trihedral reflector. The target nulls of some typical scattering characteristics are shown in Tab. 1.

Figure 1 shows how the target null is applied to reduce the contamination effect of a strong scattering point. In Fig. 1a, there are three scattering points. $s_{1,\mathrm{HH}}$ represents

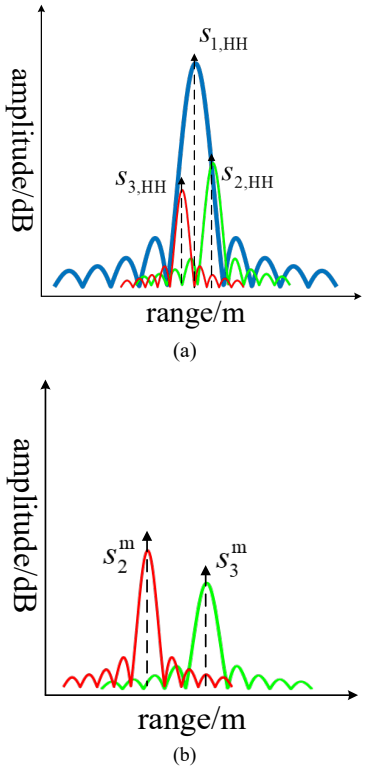


**Fig. 1.** Strong scattering point suppression in a radar image: (a) Strong scattering point contamination. (b) After processing the target nulls.

| Sac | PSM | CO-pol Null | X-pol Null |
|---|---|---|---|
| Trihedral reflector | $\begin{bmatrix}1 & 0\\0 & 1\end{bmatrix}$ | $\frac{1}{\sqrt{2}}\begin{bmatrix}1 & \pm j\end{bmatrix}^{T}$ | Arbitrary linear polarization |
| Dihedral reflector | $\begin{bmatrix}1 & 0\\0 & -1\end{bmatrix}$ | $\frac{1}{\sqrt{2}}\begin{bmatrix}1 & \pm 1\end{bmatrix}^{T}$ | $\frac{1}{\sqrt{2}}\begin{bmatrix}1 & \pm j\end{bmatrix}^{T}$ |
| Horizontal dipole | $\begin{bmatrix}1 & 0\\0 & 0\end{bmatrix}$ | $\begin{bmatrix}0 & 1\end{bmatrix}^{T}$ | $\begin{bmatrix}1 & 0\end{bmatrix}^{T}$ |
| Vertical dipole | $\begin{bmatrix}0 & 0\\0 & 1\end{bmatrix}$ | $\begin{bmatrix}1 & 0\end{bmatrix}^{T}$ | $\begin{bmatrix}0 & 1\end{bmatrix}^{T}$ |
| Cylinder | $\begin{bmatrix}2 & 0\\0 & 1\end{bmatrix}$ | $\frac{1}{\sqrt{3}}\begin{bmatrix}1 & \pm\sqrt{2}j\end{bmatrix}^{T}$ | $\begin{bmatrix}1 & 0\end{bmatrix}^{T}, \begin{bmatrix}0 & 1\end{bmatrix}^{T}$ |
| Narrow dihedral | $\begin{bmatrix}2 & 0\\0 & -1\end{bmatrix}$ | $\frac{1}{\sqrt{3}}\begin{bmatrix}1 & \pm\sqrt{2}\end{bmatrix}^{T}$ | $\begin{bmatrix}1 & 0\end{bmatrix}^{T}, \begin{bmatrix}0 & 1\end{bmatrix}^{T}$ |
| 1/4 wave device | $\begin{bmatrix}1 & 0\\0 & j\end{bmatrix}$ | $\frac{1}{\sqrt{2}}\begin{bmatrix}1 & \pm\frac{1+j}{\sqrt{2}}\end{bmatrix}^{T}$ | $\begin{bmatrix}1 & 0\end{bmatrix}^{T}, \begin{bmatrix}0 & 1\end{bmatrix}^{T}$ |
| Left-hand helix | $\begin{bmatrix}1 & j\\j & -1\end{bmatrix}$ | $\frac{1}{\sqrt{2}}\begin{bmatrix}1 & j\end{bmatrix}^{T}$ | $\frac{1}{\sqrt{2}}\begin{bmatrix}1 & j\end{bmatrix}^{T}$ |
| Right-hand helix | $\begin{bmatrix}1 & -j\\-j & -1\end{bmatrix}$ | $\frac{1}{\sqrt{2}}\begin{bmatrix}1 & -j\end{bmatrix}^{T}$ | $\frac{1}{\sqrt{2}}\begin{bmatrix}1 & -j\end{bmatrix}^{T}$ |

**Tab. 1.** Target nulls of some typical scattering characteristics.

the PSM element in the HH channel of the strong scattering point. $s_{2,\mathrm{HH}}$ and $s_{3,\mathrm{HH}}$ represent the PSM elements of two weak scattering points. Because the PSF of a strong scattering point contaminates its surrounding points, the positions of weak scattering points cannot be extracted accurately. In Fig. 1b, $s_2^{\mathrm{m}}$ and $s_3^{\mathrm{m}}$ are the measured scattering intensities after processing the target nulls. The strong scattering point is removed after processing the target nulls. The positions of the weak scattering points are acquired.

## 2.2 PSF Correction Perturbation Equations of Adjacent Scattering Points

Because target null theory helps us eliminate the effects of strong scattering points in certain polarimetric channels, we can obtain the locations of weak scattering points. However, the phenomenon in Fig. 2 still exists in other polarimetric channels. The PSFs of strong scattering points result in inaccurate values in the extracted PSMs, especially for the sidelobes of the PSFs among adjacent scattering points. Thus, it is necessary to fix the extracted polarimetric scattering matrices of adjacent scattering points.

It is reasonable to assume that the number of scattering points in the image is $N$. The influences of the PSFs among different scattering points are as follows:

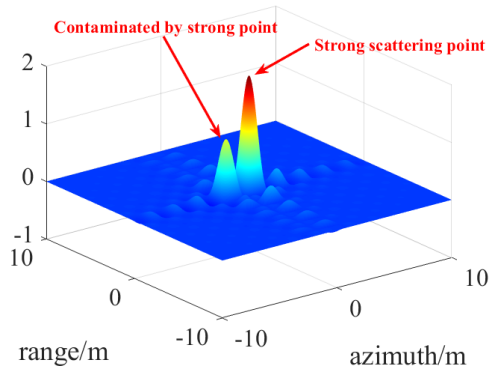


**Fig. 2.** Sidelobe contamination of two-dimensional PSF.

$$\mathbf{F}=\begin{bmatrix} f(l_{11}) & f(l_{12}) & \cdots & f(l_{1N}) \\ f(l_{21}) & f(l_{22}) & \cdots & f(l_{2N}) \\ \vdots & \vdots & \ddots & \vdots \\ f(l_{N1}) & f(l_{N2}) & \cdots & f(l_{NN}) \end{bmatrix}. \tag{8}$$

In (8), $f(\cdot)$is the normalized point spread function and $l_{ij}$, $i \neq j = 1,2,\ldots,N$ represents the relative distance between every two scattering points. If the radar transmits and receives linear frequency modulation (LFM) signals, the point spread function in the imaging process is approximated as a two-dimensional sinc function. The measured values are as follows:

$$\mathbf{x}_C = \begin{bmatrix} x_{C,1} & x_{C,2} & \cdots & x_{C,N} \end{bmatrix}^{\mathrm{T}} \tag{9}$$

where $\mathbf{x}_{C,i}(i = 1,2,\ldots,N)$ is the measured value of each scattering point in polarimetric channel $C$ = HH, HV, VH, and VV. The fixed elements of the PSMs in polarimetric channel $C$ are as follows:

$$\hat{\mathbf{S}}_C = \begin{bmatrix} \hat{s}_{C,1} & \hat{s}_{C,2} & \cdots & \hat{s}_{C,N} \end{bmatrix}^{\mathrm{T}}. \tag{10}$$

The PSF perturbation correction equations of the adjacent scattering points are expressed in matrix form as follows:

$$\mathbf{F}\hat{\mathbf{S}}_C = \mathbf{x}_C. \tag{11}$$

The coefficient matrix **F** is symmetric. Therefore, it is easy to use the eigenvalues of **F** to decide whether it is ill-conditioned. The solution is:

$$\hat{\mathbf{S}}_C = \mathbf{F}^{-1}\mathbf{x}_C, C = \mathrm{HH,HV,VH,VV}. \tag{12}$$

## 2.3 Novel Scattering Characteristic Extraction Method

A flow chart of the proposed extraction method is presented in Fig. 3:

1) The scattering characteristics of strong scattering points should be preliminarily extracted.

In this step, the radar should obtain the echo data with the H-V basis. A threshold should be set to define the intensity of the strong scattering point. The locations and PSMs of the strong scattering centers can be extracted directly.

2) The target null should be selected according to the extracted strong scattering characteristic in the CO-pol or X-pol channels.

After obtaining the PSMs of the strong scattering points, the target null of one selected scattering characteristic should be calculated.

3) After mitigating a strong scattering characteristic, the accurate locations of some weak scattering points should be extracted.

Since some strong scattering centers have been eliminated, the weak scattering centers around them can be seen and their locations can be extracted.

4) Correction equations can be established and solved to fix the extracted scattering characteristic.

Given the locations of some weak scattering points, the influence of the PSFs in the radar image should be considered. Correction equations can be established to fix the PSM, and the effects of the PSFs in the radar image can be mitigated.

5) Target decomposition is applied to analyze the extraction results.

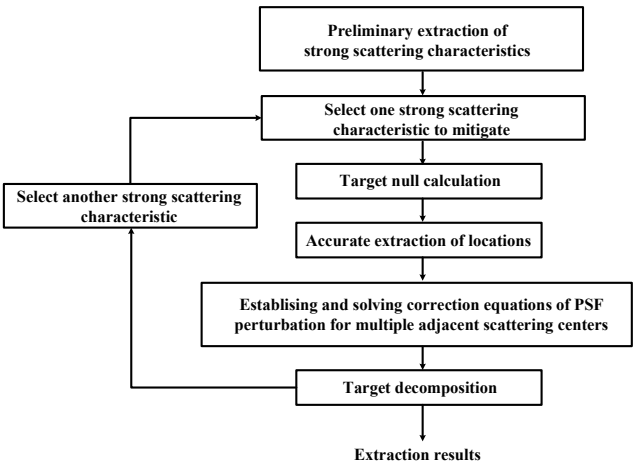


**Fig. 3.** Flow chart of the proposed method.

In this step, target decomposition is used to match the extracted PSMs with the typical scattering characteristics. The decomposition results can retrieve the geometric structure of the radar target. Cameron decomposition is applied in this paper.

6) The above procedures are repeated for different strong scattering characteristics.

Since we select only one kind of strong scattering characteristic in step 2), other target nulls of strong scattering centers should be calculated. Steps 3) to 5) are repeated for the other scattering characteristics.

# 3. Numerical Simulation

## 3.1 Simple Scenario

The first simulation involves studying the contamination impacts of strong scattering points. The two targets are shown in Fig. 4(a). The dihedral reflector is composed of two squares with a side length of 2 m. The radius of the cylinder is 1 m and its length is 4 m. Plane waves are used to illuminate the two targets. The scanning frequency range is 10 GHz–10.15 GHz. The scanning azimuth angle range is 45°–45.86°. Figure 4(b) shows the geometric centers of the two targets in the imaging axis. In the simulation, the threshold of the scattering center intensity is set as 10.

The imaging results on the H-V basis are shown in Fig. 5. In Figs. 5(a) and 5(d), the bright areas represent the dihedral reflector. In Fig. 5(b) or 5(c), the two points are the vertices of the dihedral reflector. Due to the contamination from the strong scattering center generated by dihedral reflector, we cannot obtain the location or PSF of the cylinder from the original data.

According to Tab. 1, the X-pol channel of the 45-degree linear polarization is used to mitigate the intensity of the dihedral reflector. The imaging results are shown in Fig. 6.

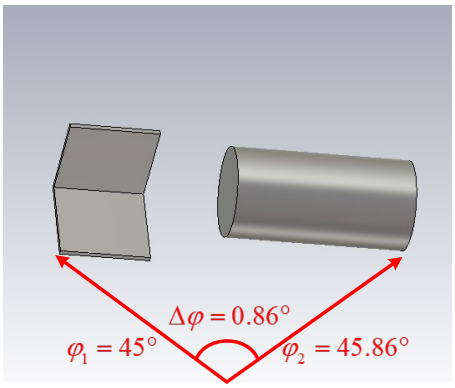


(a)

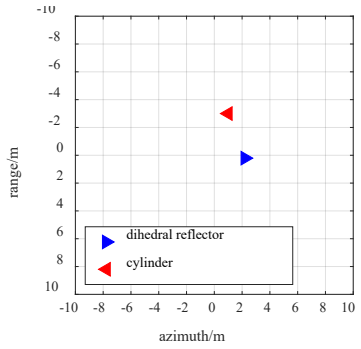


(b)

**Fig. 4.** The cylinder and the dihedral reflector utilized in the simulation: (a) Simulation targets. (b) Geometric centers on the imaging axis.

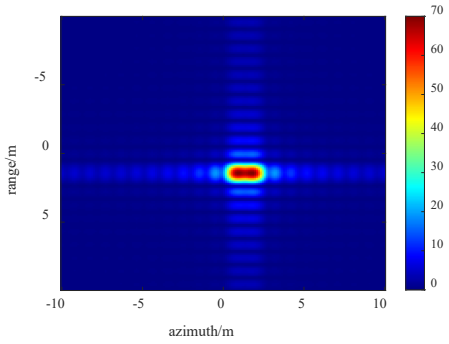


(a)

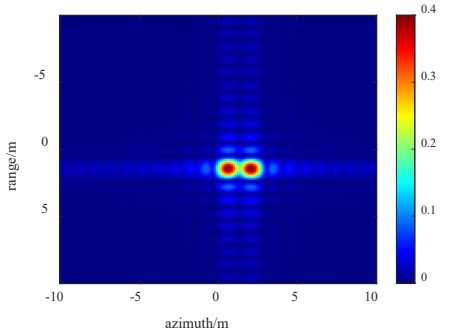


(b)

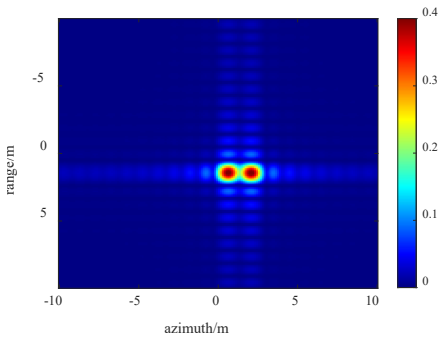


(c)

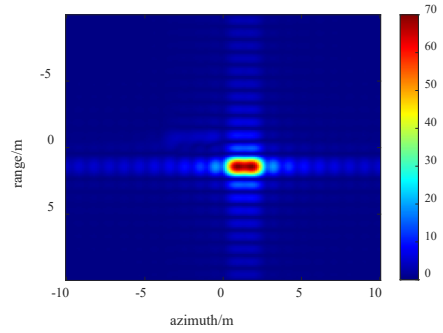


(d)

**Fig. 5.** Imaging results with the H-V basis of two targets: (a) HH channel, (b) HV channel, (c) VH channel, (d) VV channel.

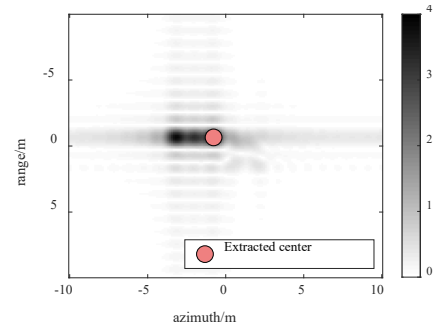


(a)

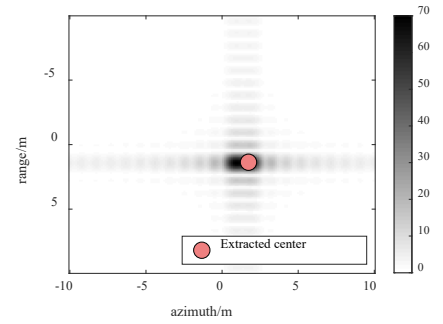


(b)

**Fig. 6.** Imaging results of the target null selection process: (a) 45-degree linear CO-pol channel, (b) 45-degree linear X-pol channel.

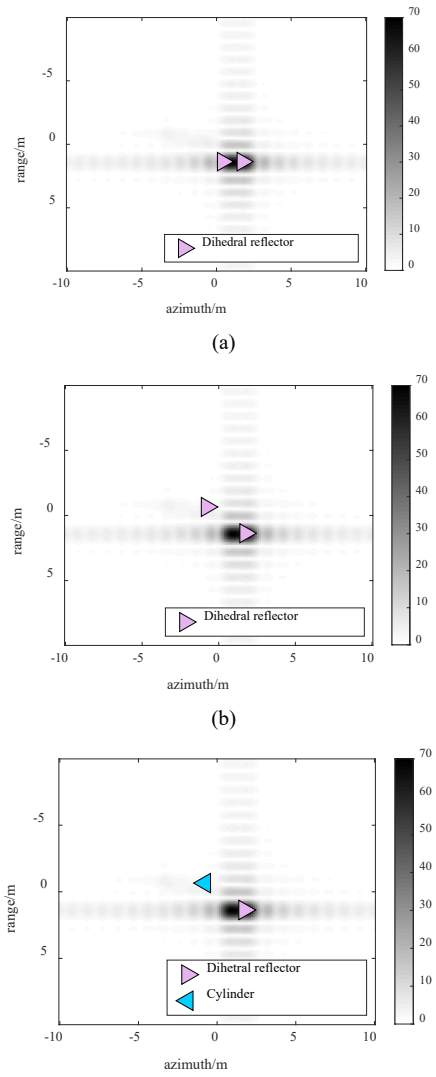


**Fig. 7.** Cameron decomposition results of the two targets: (a) Extraction using the original data. (b) Extraction without correction. (c) Extraction after correction.

In Fig. 6(a) and 6(b), the two black areas represent the cylinder and dihedral reflector, respectively. The two extracted scattering center locations that appear after target null processing are marked. After obtaining the locations, the aforementioned correction equations are applied to fix the measured values of the PSMs. Figure 7 shows the Cameron decomposition results of the extracted PSMs.

Figure 7(a) shows the extraction results gathered from the original data with the H-V basis. There are two scattering centers on the one dihedral reflector. In Fig. 7(b), it is shown that if we do not fix the extracted PSMs, most of the targets are recognized as dihedral reflectors. In Fig. 7(c), it is shown that the cylinder is extracted accurately.

## 3.2 Multiple Targets

The second simulation involves performance tests of the proposed method for multiple targets. The adjacent targets used in the simulation are shown in Fig. 8, which

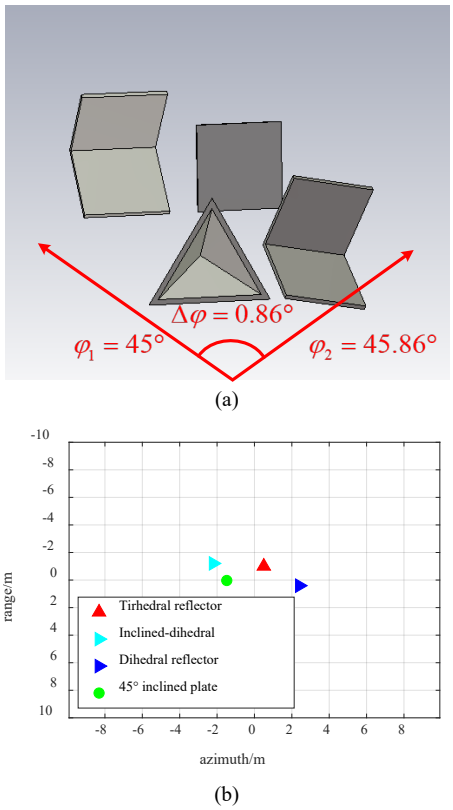


**Fig. 8.** Four reflectors used in the simulation: (a) Multiple targets scene. (b) Geometric centers in the imaging axis.

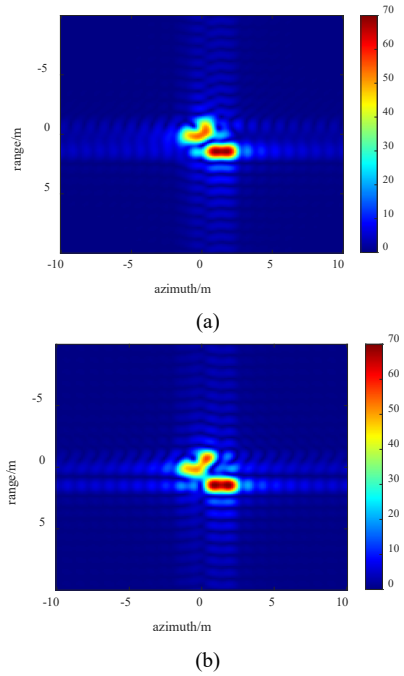


**Fig. 9.** Radar images of the CO-pol channels with the H-V polarimetric basis: (a) HH, (b) VV.

includes two dihedral reflectors, one trihedral reflector and a 45° inclined plate. The dihedral and plate reflectors are composed of squares with side lengths of 2 m. One dihedral reflector has a 20-degree inclination angle. The trihedral reflector is composed of isosceles right triangles with

right-angle side lengths of 2 m. In addition, plane waves are used. The scanning frequency and angle parameters are the same as those in the simulation in Sec. 3.1. The four targets are shown in Fig. 8.

For CO-pol channels with the H-V basis, Figures 9(a) and 9(b) show that the location of the inclined dihedral reflector cannot be accurately extracted due to the PSF contamination of the strong scattering centers generated by the trihedral reflectors in the azimuth and range.

For the 20-degree-inclined dihedral reflector, its PSM can be calculated as follows:

$$\begin{aligned}\mathbf{S}_{\mathrm{Dih}}(\theta)\big|_{\theta=20^\circ} &= \mathbf{R}(\theta)\mathbf{S}_{\mathrm{Dih}}\mathbf{R}^{\mathrm{T}}(\theta)\big|_{\theta=20^\circ} \\ &= \begin{bmatrix}\cos 20^\circ & \sin 20^\circ \\ -\sin 20^\circ & \cos 20^\circ\end{bmatrix}\begin{bmatrix}1 & 0 \\ 0 & -1\end{bmatrix}\begin{bmatrix}\cos 20^\circ & -\sin 20^\circ \\ \sin 20^\circ & \cos 20^\circ\end{bmatrix} \\ &= \begin{bmatrix}-\cos 40^\circ & \sin 40^\circ \\ \sin 40^\circ & \cos 40^\circ\end{bmatrix}\end{aligned} \tag{13}$$

where $\mathbf{S}_{\mathrm{Dih}} = \begin{bmatrix}1 & 0 \\ 0 & -1\end{bmatrix}$ is the PSM of dihedral reflector, $\mathbf{R}(\theta) = \begin{bmatrix}\cos\theta & \sin\theta \\ -\sin\theta & \cos\theta\end{bmatrix}$ is the rotation matrix, and $\theta$ is the attitude angle. Because the secondary diagonal elements of the PSM are not zero, H- and V- polarized waves are used in the X-pol channel to mitigate other reflectors. Figure 10 shows the imaging results of the X-pol channels with the H-V basis.

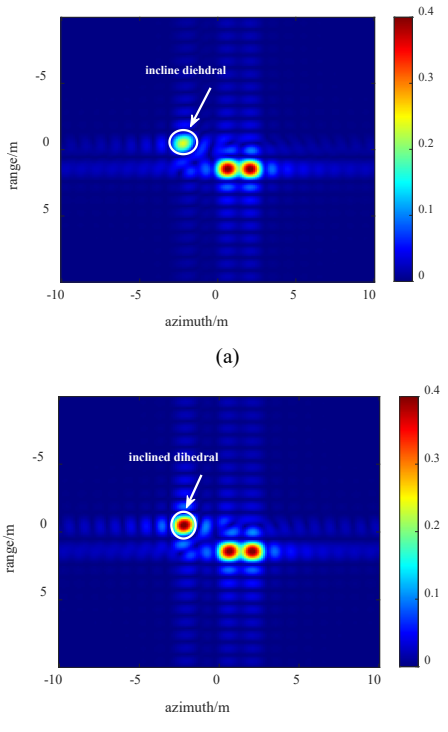


**Fig. 10**. Radar images of the X-pol channels under the H-V polarimetric basis: (a) VH, (b) HV.

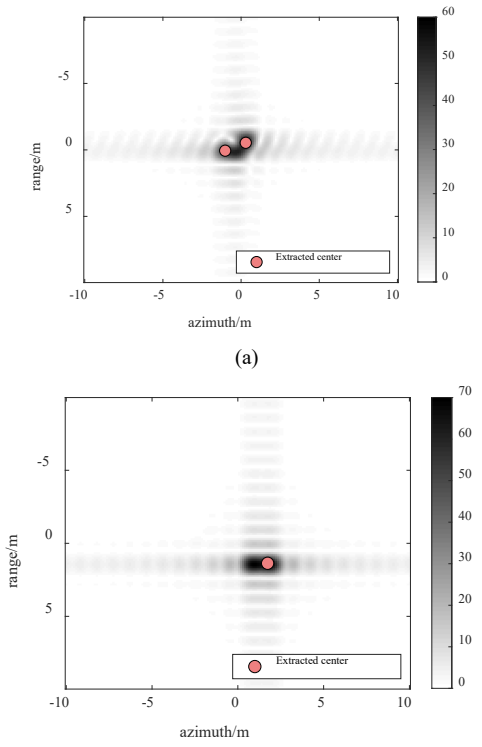


**Fig. 11.** Imaging results of the target null selection process: (a) 45-degree linear CO-pol channel. (b) 45-degree linear X-pol channel.

Figure 10 shows that the two points in the upper left represent the 20-degree-inclined dihedral reflector. The scattering intensity of the dihedral reflector is mitigated by its inclination. The other bright areas are the vertices of the dihedral reflector. Figure 11 shows the images after processing the target nulls and the extracted points. After suppressing the scattering intensity levels of the dihedral characteristics, images are taken and the results are shown in Fig. 11(a). In Fig. 11(b), due to the mitigation of the trihedral characteristic, there is only one bright area. The locations of the other scattering centers are extracted.

Figure 12(a) shows the decomposition results generated by the original data with the H-V basis after acquiring the locations of the scattering centers. There are two scattering centers on the dihedral reflector. Only one trihedral characteristic can be extracted accurately. In Fig. 12(b), if we do not fix the extracted PSMs, the upper trihedral reflector is recognized as a dihedral reflector. In Fig. 12(c), we find that the upper trihedral reflector is extracted accurately. For the 20-degree-inclined dihedral reflector in the upper left, its PSM is decomposed as a 1/4 wave device. Therefore, the performance of the proposed method is limited for nonorthogonal targets.

Figure 13 shows that the extracted positions are not totally in accord with their geometric centers. This result is a byproduct of the radar imaging algorithm and the scattering behaviors among the reflectors. This phenomenon is not caused by the proposed method. In Fig. 13, it is seen that most of the extracted positions are within the geomet-

ric outline and the extracted locations are changed by the observation angle of the radar.

From the simulations in Sec. 3.1 and 3.2, after processing the target nulls, the effects of the strong scattering centers are eliminated and the weak scattering characteristics are extracted accurately.

## 3.3 Complex Manmade Target

In this section, a simulation involving a satellite model is used to demonstrate the performance of the proposed method. The satellite model is shown in Fig. 14.

In this simulation, we use plane waves to illuminate the satellite. The scanning range of the azimuth angle is –8° to 8°. The frequency range is 9 GHz–12 GHz. The inverse synthetic aperture radar (ISAR) images with the H-V basis are shown in Fig. 15.

In Fig. 15, most of the geometric structures of the satellite model cannot be seen. Only the strong scattering centers are highlighted. These strong scattering centers are extracted directly in Fig. 16.

In Fig. 16, the strong scattering centers are extracted and the Cameron decomposition results demonstrate that the strong scattering centers are generated by the trihedral reflectors and helix structures. Therefore, these strong scattering centers are mitigated by transmitting and receiving left-hand circular/right-hand circular (LHC/RHC) polarized waves. The imaging results with a circular polarization basis are shown in Fig. 17.

In Fig. 17(a), the main geometric structure of the satellite model is clearly visible because both the intensities of the trihedral reflectors and the helix structures are suppressed in the CO-pol channel of the LHC polarized waves. However, in Fig. 17(b), when the radar antenna transmits LHC-polarized waves and receives RHC-polarized waves, the strong scattering points representing the helix structures are suppressed, however, the strong scattering points representing the trihedral reflectors are retained. From Fig. 17(a), the positions of these strong and weak scattering points are extracted and the Cameron decomposition results are obtained, as shown in Fig. 18.

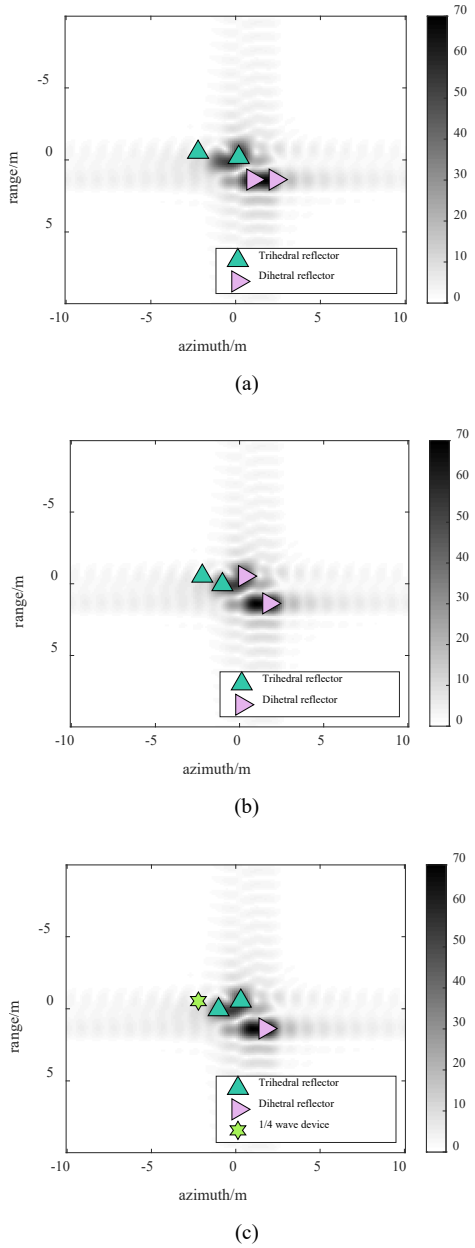


**Fig. 12.** Cameron decomposition results: (a) Extraction using original data. (b) Extraction without correction. (c) Correction results for the HH image.

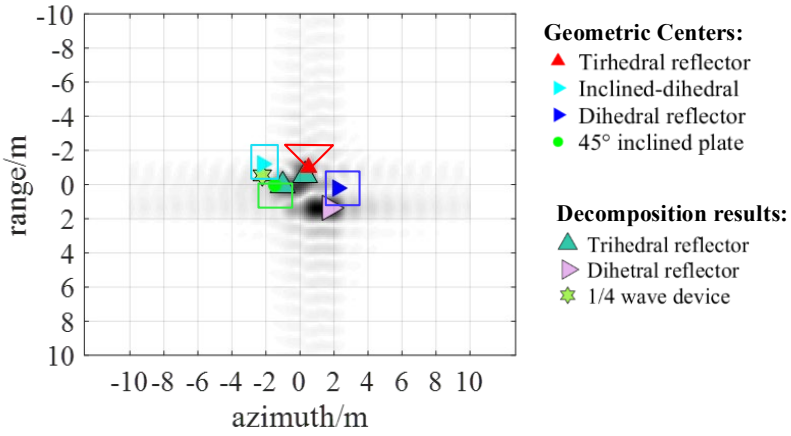


**Fig. 13.** Geometric outlines of the reflectors and extracted points.

In Fig. 18, the main scattering characteristics of the satellite model are mainly composed of trihedral reflectors and helix structures. The scattering characteristics in solar cell panel are mainly 1/4 wave devices and dipoles. Moreover, the rounded corners of some solar panel joints are decomposed into cylinders. This figure indicates that some weak scattering characteristics are correctly extracted after target null processing and the proposed method is effective.

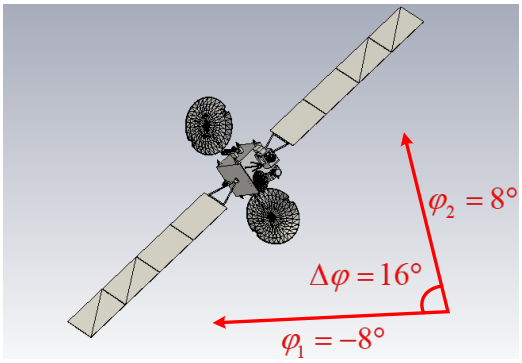


**Fig. 14.** Satellite model.

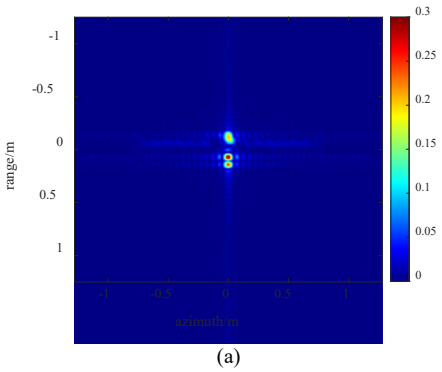


(a)

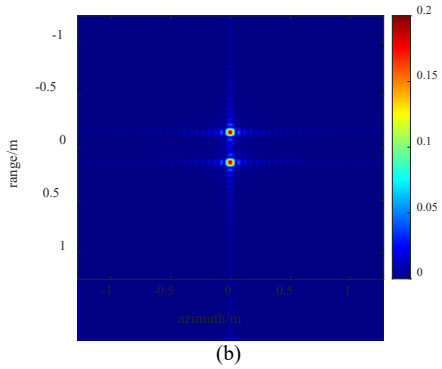


(b)

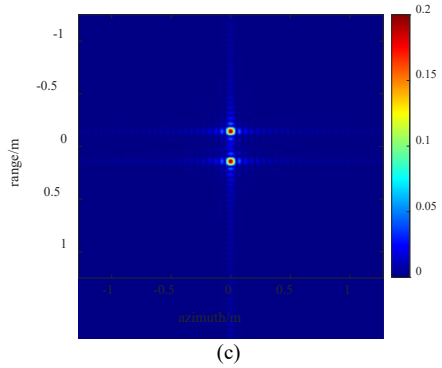


(c)

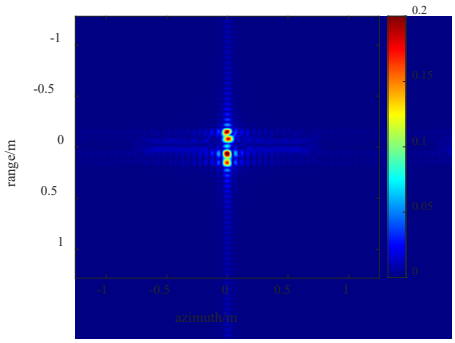


(d)

**Fig. 15.** Imaging results with the H-V basis of satellite model. (a) HH channel, (b) HV channel, (c) VH channel, (d) VV channel.

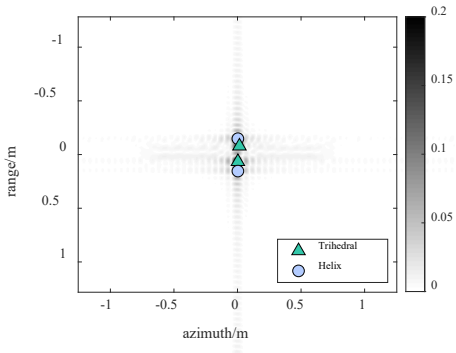


**Fig. 16.** Strong scattering centers of the satellite model.

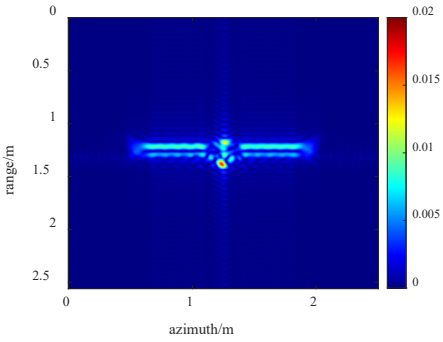


(a)

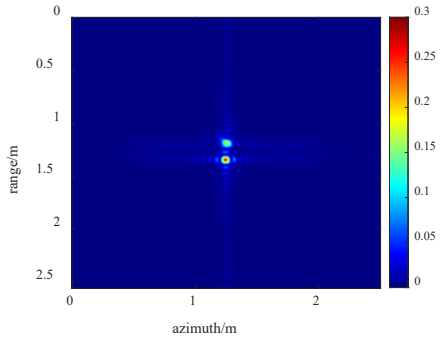


(b)

**Fig. 17.** Imaging results with circular polarization basis of the satellite model: (a) CO-pol channel of LHC. (b) X-pol channel of LHC.

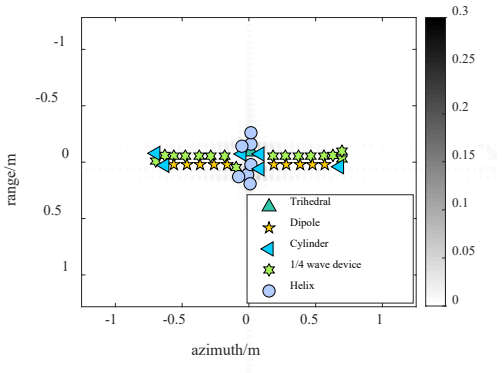


**Fig. 18.** Cameron decomposition results of the satellite model.

## 4. Measurement Data Discussion

To further verify the accuracy of the weak scattering characteristic extraction method proposed in this paper, the measurement data of Gaofen-3 is used. The data are obtained with the fully polarized strip mode in the C band. Both the range and azimuth resolution are 5 m. The imaging result of a cargo ship with an H-V polarization basis is shown in Fig. 19.

In Fig. 19(a) and 19(d), the geometric structure of the cargo ship is not clearly displayed because of the contamination of the strong scattering centers. Although Figures 19(b) and 19(c) show parts of the ship structures, there are still strong scattering centers and the intensities of the other scattering centers are not uniform. These strong scattering centers are extracted and the Cameron decomposition results are shown in Fig. 20.

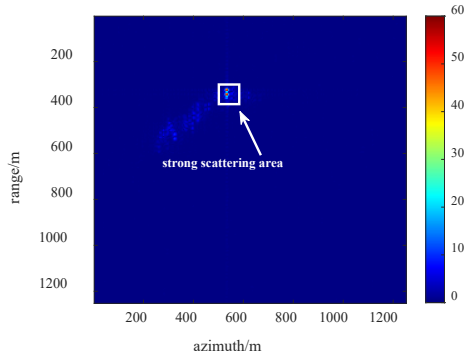


(a)

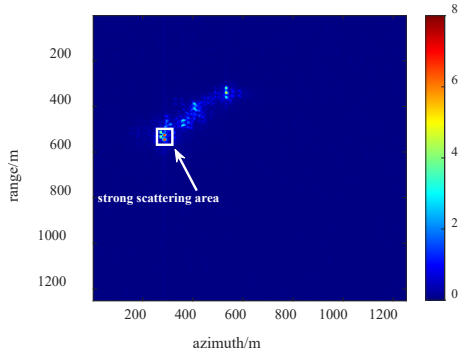


(b)

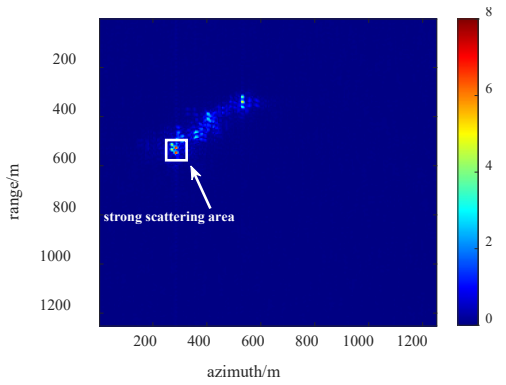


(c)

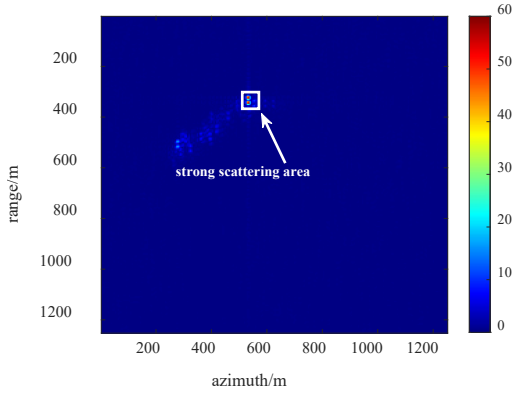


(d)

**Fig. 19.** Imaging results of the cargo ship with the H-V basis: (a) HH, (b) HV, (c) VH, (d) VV.

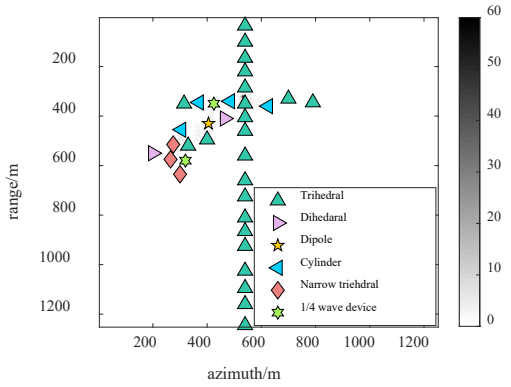


**Fig. 20.** Cameron decomposition results of the cargo ship with the H-V basis.

According to Fig. 19 and Fig. 20, the strong scattering points caused by the trihedral reflectors are the main factors affecting the weak scattering characteristics of the cargo ship. The strong scattering points of the cargo ship generate many obvious side lobes in the range axis of the radar image. Therefore, it is necessary to use the target null method proposed in this paper to eliminate them and the imaging result is shown in Fig. 21.

In Fig. 21, the strong scattering centers caused by the trihedral reflectors are greatly mitigated, and the cargo ship outline is shown more clearly in the radar image. Moreover, the amplitudes of the scattering centers are more uni-

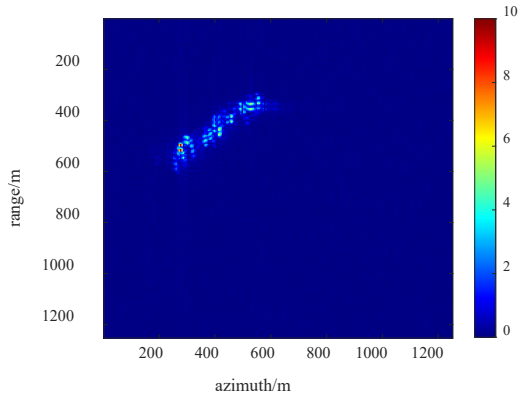


**Fig. 21.** Imaging result of 45-degree linear X-pol channel.

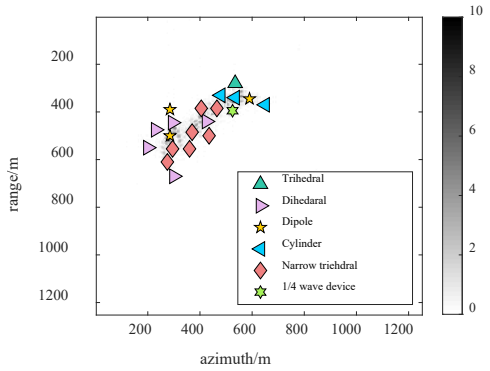


**Fig. 22.** Cameron decomposition results of the cargo ship after processing target nulls.

form. The positions of the weak scattering centers are extracted to obtain the Cameron decomposition results shown in Fig. 22.

After suppressing the effects of the strong scattering centers shown in Fig. 19, more scattering points with dihedral and narrow dihedral reflector characteristics are shown in Fig. 22, corresponding to the dihedral reflectors between the containers and the bridge deck structures. An analysis of the measured Gaofen-3 data also demonstrates that the proposed method extracts the weak scattering characteristics of the radar targets.

## 5. Conclusion

The foundation of polarimetric radar target recognition processes lies in the effective extraction of scattering characteristics. In this paper, aiming at the problem of accurate adjacent manmade target extraction, the method of target null selection for scattering characteristic extraction is proposed. The innovations of the proposed method include the following two aspects. First, the locations of the weak scattering points in the radar image are highlighted by selecting a suitable target null to mitigate the intensity levels of the strong scattering points in the CO-pol or X-pol channels. Second, after acquiring the locations of the weak scattering points in certain polarimetric channels, the components of the PSMs extracted from other polarimetric channels are fixed by solving the perturbation correction equations of the PSFs for multiple adjacent scattering centers. The electromagnetic simulation results and measurement data discussion demonstrate that the proposed method works very well when the weak target to be retrieved is orthogonal to the strong target, otherwise, the procedure leads to the removal of part of the power coming from the weak target, making its detection more challenging.

## Acknowledgments

This research is supported by the National Natural Science Foundation of China (NSFC) under grants no. 61901496 and no. 61901499.

## References

[1] CHENG, X., LI, Y. Z., WANG, X. S., et al. Research on wideband polarization correlation of spatial precession targets (in Chinese). *Radar Science and Technology,* 2015, vol. 13, no. 4, p. 425–432. DOI: 10.3969/j.issn.1672-2337.2015.04.016

[2] ZHAO, F., XU, Z. M., WU, Q. H., et al. Dynamic scattering analysis of midcourse ballistic targets with separation movements. *Journal of Radars*, 2021, vol. 10, no. 3, p. 360–369. DOI: 10.12000/JR21047

[3] XING, S. Q., LI, Y. Z., DAI, D. H., et al. Three-dimensional reconstruction of man-made objects using polarimetric tomographic SAR. *IEEE Transactions on Geoscience and Remote Sensing*, 2013, vol. 51, no. 6, p. 3694–3705. DOI: 10.1109/TGRS.2012.2220145

[4] BAI, Y., WU, Y., YIN, H. C., et al. Indoor measurement research on polarimetric scattering characteristics of UAV. *Journal of Radars*, 2016, vol. 5, no. 6, p. 647–657. DOI: 10.12000/JR16032

[5] CUI, X. C., SU, Y., CHEN, S. W. Polarimetric SAR ship detection based on polarimetric rotation domain features and superpixel technique. *Journal of Radars*, 2021, vol. 10, no. 1, p. 35–48. DOI: 10.12000/JR20147

[6] BOERNER, W., YAN, W., XI, A., et al. On the basic principles of radar polarimetry: The target characteristic polarization state theory of Kennaugh, Huynen's polarization fork concept, and its extension to the partially polarized case. In *Proceedings of the IEEE*, 1991. vol. 79, no. 10, p. 1538–1550. DOI: 10.1109/5.104228

[7] YANG, J., PENG, Y. N., YAMAGUCHI, Y., et al. Extension of the Kennaugh null theory. In *2000 5th International Symposium on Antennas, Propagation, and EM Theory (ISAPE 2000).* Being (China), 2000, p. 69–74. DOI: 10.1109/ISAPE.2000.894726

[8] YANG, J., YAMAGUCHI, Y., YAMADA, H., et al. Development of target null theory. *IEEE Transactions on Geoscience and Remote Sensing*, 2001, vol. 39, no. 2, p. 330–338. DOI: 10.1109/36.905241

[9] YANG, J., YAMAGUCHI, Y., YAMADA, H., et al. The characteristic polarization states and the equi-power curves. *IEEE Transactions on Geoscience and Remote Sensing*, 2002, vol. 40, no. 2, p. 305–313. DOI: 10.1109/36.992789

[10] MORIYAMA, T., KASAHARA, H., YAMAGUCHI, Y., et al. Advanced polarimetric subsurface FM-CW radar. *IEEE*

*Transactions on Geoscience and Remote Sensing*, 1998, vol. 36, no. 3, p. 725–731. DOI: 10.1109/36.673665

[11] YAMAGUCHI, Y., MITSUMOTO, M., SENGOKU, M., et al. Synthetic aperture FM-CW radar applied to the detection of objects buried in snowpack. In *IEEE Antennas and Propagation Society International Symposium*. Chicago (IL, USA), 1992, vol. 2, p. 1122–1125. DOI: 10.1109/APS.1992.221573

[12] CAMERON, W. L., LEUNG, L. K. Feature motivated polarization scattering matrix decomposition. In *IEEE International Conference on Radar*. Arlington (VA, USA), 1990, p. 549–557. DOI: 10.1109/RADAR.1990.201088

## About the Authors ...

**LU Dongwei** was born in 1992. He received his M.Sc. from the University of Electronics Science and Technology of China in 2017. His research interest is in the field of polarimetric radar signal processing.

**MA Jiazhi** (corresponding author) was born in 1987. He received his Ph.D. from the National University of Defense Technology in 2017. His research interest is in the field of polarimetric radar signal processing.

**PANG Bo** was born in 1984. He received his Ph.D. from the National University of Defense Technology in 2013. His research interests are in the field of polarimetric radar imaging and MIMO radar signal processing.

**GUAN Yifu** was born in 1988. He received his Ph.D. from the National University of Defense Technology in 2019. His research interests include the fields of synthetic aperture radar imaging and radar target recognition.

**FENG Dejun** was born in 1972. He is a Professor of the National University of Defense Technology. His research interests include the fields of synthetic aperture radar imaging and polarimetric radar signal processing.